3 Biotech (2023) 13:244
https://doi.org/10.1007/s13205-023-03663-3

ORIGINAL ARTICLE

Development of silver nanoparticles and aptamer conjugated biosensor for rapid detection of *E. coli* in a water sample

Ajinkya Hariram Dabhade[1] · Ravi Prakash Verma[1] · Balasubramanian Paramasivan[2] · Adhidesh Kumawat[1] · Biswajit Saha[3]

Received: 11 February 2023 / Accepted: 5 June 2023

Abstract
A simple, rapid, and sensitive electrochemical biosensor based on a screen-printed carbon electrode (SPCE) was developed for onsite detection of *E. coli* in real time. This work analyzed the effect of aptamer conjugation and PBS buffer solution on the colloidal stability of the silver nanoparticles (AgNPs). Aggregations of the AgNPs after aptamer conjugation in PBS buffer were observed from the particle size distribution analysis. The AgNP-aptamer conjugation and its affinity towards *E. coli* (DH5α) were confirmed by UV–visible spectrophotometry, which showed a linear increment in the absorption with increasing *E.coli* concentration. The screen-printed carbon electrodes were modified by drop-casting of AgNPs, which were used as an effective immobilization platform for *E. coli*-specific aptamers. The modified electrode's surface modification and redox behavior were characterized using cyclic voltammetry. Finally, *E. coli* was detected using differential pulse voltammetry with an optimized incubation time of 15 min. The developed biosensors showed a linear decrease in current intensity with an increase in the concentration of *E.* coli. The biosensor had a relative standard deviation (RSD) of 6.91% (n = 3), which showed good reproducibility. The developed biosensors are highly sensitive and have a limit of detection (LOD) as low as 150 CFU/ml. The biosensor showed good selectivity for *E.coli* coli when comparing the signal response obtained for bacteria other than *E.coli*. Also, the biosensor was found stable for four weeks at room temperature and showed high recoveries from 95.27% to 107% during the tap water sensitivity validation.

Keywords Biosensor · Electrochemical · Silver nanoparticles · Screen printed electrode · Bacteria detection

Introduction

Waterborne enteric pathogens like bacteria, viruses, and protozoa in domestic water supplies carry a significant human health risk. About 3.4 million people are globally affected, and over 1.23 million children have died of diarrhoea, mainly caused by waterborne bacteria (WHO, 2000). Also, diarrhoea causes the death of one in every ten children worldwide (WHO 2014). Traditionally, the faecal coliform bacteria have been used as an indicator organism to analyze water quality and detect pathogenic bacteria in water (U.S. Environmental Protection Agency, 1976). Sewage and animal waste can contain various disease-causing microorganisms. *Escherichia coli* (*E. coli)* is a type of faecal coliform bacterium commonly found in the intestines of animals and humans. It indicates sewage or animal waste contamination (Khan et al. 2020). Therefore, a fast and efficient sensing platform for bacteria is urgently needed for the early diagnosis of bacterial diseases.

Conventional bacterial detection employs various complex methods that include microscopy, cell culture assays, DNA sequencing, polymerase chain reaction (PCR), and enzyme-linked immunosorbent assay (ELISA) (Foddai et al. 2020). The abovementioned methods are time-consuming and costly as they involve a series of preliminary experiments like the lysis of cells and the extraction, quantification, amplification, and purification of DNA. Thus, these detection methods are associated with manual errors,

✉ Biswajit Saha
bsaha@iitgn.ac.in

[1] Department of Chemical Engineering, National Institute of Technology Rourkela, Rourkela, Odisha 769008, India

[2] Department of Biotechnology and Medical Engineering, National Institute of Technology Rourkela, Rourkela, Odisha 769008, India

[3] Department of Chemical Engineering, Indian Institute of Technology Gandhinagar, Palaj, Gujarat 382355, India

Published online: 19 June 2023

false-positive results, and expensive equipment. The coliform test is time-consuming (> 24 h) and performed by skilled staff in well-equipped laboratory conditions (Elmund et al. 1999; Shen et al. 2019).

The next generation of analytical detection techniques biosensors comprises an integrative arrangement of biochemical and physiochemical detection methods and are employed for regular surveillance in food processing industries. It's a simple, fast, and sensitive technique to detect several foodborne pathogens, compared to the other complicated commercial methods. This biosensor technology can be successfully implemented to reduce the previously mentioned efforts and assay time. A biosensor is a device that generates measurable signals by integrating transducer elements with receptors like tissue, microorganisms, cells, antibodies, enzymes, nucleic acids, aptamers, bacteriophages, etc. (Templier et al. 2016). A bioreceptor recognizes the target analyte and a transducer converts the recognition event into a measurable electrical signal. The amplifier receives the electrical signal transmitted from the transducer and converts it into the required waveforms. The processor then analyzes the stored amplified signal and displays it as an output. The detection is purely based on the intrinsic properties of the analytes, such as charge, molecular weight, dielectric permittivity, electrical impedance, etc.

Label-free biosensing technologies have made enormous progress in recent years, as they are inexpensive, rapid, and require much less reaction volume. Recent developments in nanotechnology and its implementation in sensing methodologies are promising approaches to improving the performance of biosensors. At the same time, advancements in micro- and nanofabrication methods resulted in compatible miniature devices for onsite applications (Vikesland 2018). Noble metals like gold and silver nanoparticles have been extensively studied for sensor and imaging applications. Generally, these metals are chemically inert but possess unique physicochemical properties at the nanoscale (Wu et al. 2011). The physical and electrochemical changes that occur due to the binding of the biorecognition agent on the surface of nanoparticles define the role of metal nanoparticles (MNPs). Depending on their properties and functionalities, these MNPs can be used as an immobilizing platform (Sabouri et al. 2014), an electron transfer accelerator (Li et al. 2010), a catalyst for chemiluminescence reactions (Zhong et al. 2014), a refractive index modifier (Sugawa et al. 2015), or an amplifier for mass change (Yan et al. 2015).

Silver nanoparticles (AgNPs) are the fascinating nanoparticles used in biosensing applications among several metal nanoparticles. AgNPs have been used as transducers that facilitate electron exchange on the electrode surface and produce measurable signals proportional to the concentration of analytes. The AgNPs-based sensing platform has made significant progress in monitoring the environment and food quality because of its high sensitivity and excellent biocompatibility (De and Kalita 2021). Over the last two decades, efforts have been made toward developing novel analytical methods for detecting pathogens using AgNPs and their nanocomposites. Zheng et al. (2018) developed a mercapto phenylboronic acid functionalized AgNPs-based colorimetric sensor to detect bacteria. Yu et al. (2020) developed an aptamer-based high-throughput colorimetric biosensor for detecting S. aureus with a detection limit of 81 CFU/ml.

Although colorimetric detection is highly sensitive, the requirements of a UV–visible spectrophotometer and immunoassay analyzer prove a limitation for its use in remote areas. Also, this process involves several steps that extend the assay time. Mathelie-Guinlet et al. (2019) demonstrated a voltammetric biosensor for detecting *E. coli* using polyclonal antibodies as a recognition agent immobilized on silica nanoparticles on a modified gold electrode. The biosensor had a response time of 30 min and a considerably high limit of detection (LOD) of 10^3 CFU/ml, limiting the applicability of the sensor. Altintas et al. (2018) detected *E. coli* with a LOD of 50 CFU/ml by developing antibody- and enzyme-based microfluidic biosensors.

Antibodies cannot remain stable over a wide range of pH and temperature compared to nucleic acids. Aptamers have advantages over enzymes and antibodies due to their high specificity and robustness; thus, aptamers are widely used as recognition agents in different biosensor developments. A sandwich-type aptamer-based electrochemical immunosensor was demonstrated by Bu et al. (2020) for detecting a pathogenic strain of *E. coli* at a low concentration of 32 CFU/ml. The authors have described the modification of gold electrodes with DNA aptamers specific to *E. coli O157:H7*. The binding of methylene blue-magainin I nanocomposite to the captured *E. coli* cells causes a change in the current signals, which is analyzed by cyclic voltammetry (CV) and differential pulse voltammetry (DPV).

Several authors illustrated the modification of screen-printed electrodes (SPEs) based electrochemical biosensors for bacteria detection. Siller et al. (2020) modified the screen-printed gold electrode by immobilizing an *E. coli*-specific aptamer to develop an impedimetric biosensor. Screen-printed carbon electrodes (SPCEs) modified using single-walled carbon nanotubes for facilitating the self-assembly of the *E. coli*-specific aptamer were illustrated by Housaindokht et al. (2018). Also, SPCEs were modified with a nanocomposite of boron–carbon nanorods and nickel nanoparticles to increase the sensitivity and immobilize *E. coli*-specific aptamers through poly-lysine linking (Kaur et al. 2020). Conventional gold and glassy carbon electrodes lose their functionality over time due to repetitive use, and their replacement could be more affordable. SPEs can overcome this issue as these are one-time-use disposable electrodes,

proving a better alternative to the costly and bulky conventional electrodes. However, the complex procedure for modifying electrodes involves expensive chemicals and multiple steps, which increases fabrication and assay costs. Developing a simple and effective SPCE modification method is essential to addressing the above issues.

The present work demonstrates the modification of SPCEs using AgNPs as an immobilizing platform for *E. coli*-specific DNA aptamers and an effective transducing element for detecting bacteria in water samples. The differential pulse voltammetry method was used with optimized parameters to analyze electrochemical sensing and the functionality of the developed biosensor. The developed biosensor is highly sensitive and can detect a concentration of bacteria as low as 150 CFU/ml in an optimum response time of 15 min. The calibration studies of the biosensor were performed at standard conditions using 10 mM phosphate buffer saline at pH 7.4, whereas validation studies were done using spiked tap water samples. The proposed biosensor showed good recovery, reproducibility, and stability.

Materials and methods

E. coli DH5α strain was obtained from MTCC, India. A thiol (SH) modified single-stranded DNA aptamer of the sequence below (Kim et al. 2013) was purchased from Eurofins.

5′GCAATGGTACGGTACTTCCGTTGCACTGTGCGG CCGAGCTGCCCCCTGGTTTGTGAATACCCTGGGCAA AAGTGCACGCTACTTTGCTAA3′ (90-mer).

A resuspension buffer of pH 7.4 was added to the commercially synthesized aptamer, and aliquots were preserved at −20 °C. Screen-printed carbon electrodes were purchased from Zensor. Silver nitrate, sodium borohydride, polyvinylpyrrolidone (PVP), KCl, NaCl, KH_2PO_4, Na_2HPO_4, $MgCl_2$, potassium ferrocyanide, potassium ferricyanide, Tris HCl, ethylene diamine tetraacetic acid (EDTA), and tris-(2-carboxyethyl)-phosphine (TCEP-HCl) were purchased from Sigma-Aldrich. LB broth and agar powder were purchased from Himedia. A 10 mM stock solution of $AgNO_3$ was prepared by adding 170 mg of $AgNO_3$ to DI water, and the stock was diluted 10 times to get a solution of 1 mM. Sodium borohydride 20 mM stock was prepared by adding 75 mg in 100 ml, and then it was diluted to a 3 mM concentration (4.5 ml of the 20 mM solution was added to 25.5 ml of DI water). 0.3% (w/v) PVP was prepared by adding 60 mg to 20 ml of DI water. Phosphate buffer saline (PBS) pH 7.4 (folding buffer) was prepared by adding 4 g NaCl, 0.1 g KCl, 0.72 g Na_2HPO_4, 0.123 g KH_2PO_4, and 0.047 g $MgCl_2$ (1 mM) to 300 ml of DI water. pH was adjusted to 7.4 using 0.1 N HCl, and DI water was added to make 500 ml as the final volume. Tris–EDTA (TE) buffer (resuspension buffer) was prepared by adding 0.121 g Tris HCl (10 mM) and 0.038 g EDTA (0.1 mM) in 60 ml DI water. pH was adjusted to 7.4 using 0.1 N HCl, and DI water was added to make the final volume of 100 ml.

Preparation of known *E. coli* concentration

The *E. coli* culture was grown overnight in LB broth at 37 °C and diluted 10 times in PBS buffer at pH 7.4. The culture was centrifuged, and the pellet was resuspended in a PBS buffer. The concentration was calculated by serial dilutions and colony counting on the agar plate. 100 µl of 10^{-5} diluted culture stock was plated on agar plates under a laminar biosafety cabinet and kept for 24 h. The *E. coli* concentration was calculated from Eq. 1.

$$\mathrm{CFU/ml} = \frac{\textit{Sum of the number of colonies counted}}{\textit{Number of plates} \times \textit{Volume of culture plated in ml} \times \textit{Dilution}} \quad (1)$$

Synthesis of silver nanoparticles (AgNPs)

A 30 ml of a 3 mM sodium borohydride solution was kept in an ice bath for 15 min under continuous stirring. After that, 5 ml of 1 mM silver nitrate solution was added dropwise slowly (approximately one drop per second) and mixed continuously until the solution turned colorless to faint yellow. Then, 1 ml of 0.3% (w/v) PVP was added as a stabilizer, and the solution was stirred continuously for about 30 min. Finally, the sample was preserved in an amber glass bottle at 4 °C for future use. The synthesized AgNPs were characterized using a transmission electron microscope (TEM), UV–visible spectroscopy, dynamic light scattering (DLS), and a zeta potential analyzer.

Aptamer-AgNP conjugation

A PBS buffer containing 5 mM $MgCl_2$ (refolding buffer) was added with the thiol-modified aptamer to prepare the final concentration of 5 µM aptamer. The solution was heated at 90–95 °C for 5 min to refold the single-stranded DNA aptamer and cooled to room temperature. 200 µl of 5 µM aptamer was incubated with 20 µl of 5 mM TCEP in the dark box for 1 h. Later, the solution was added to 1 ml of AgNPs, which made the final concentration of the aptamer 1 µM. The solution was then incubated in the dark box at room temperature for 24 h. Then, the solution was centrifuged at 13,000 rpm for 30 min, and the pellet was washed with DI water. These washing steps were repeated three times. After that, the pellet was resuspended in DI water for storage.

Circular dichroism analysis

The secondary structure of the aptamer-conjugated AgNPs present was analyzed using circular dichroism (CD) spectrometry with JASCO (J1 500) at 300 to 200 nm wavelength. A 5 µM aptamer in 10 mM PBS buffers of pH 7.4 was used as a standard sample for comparative analysis.

UV–visible spectroscopy analysis

A 100 µl of aptamer-conjugated AgNPs solution was added to 900 µl of PBS buffer to prepare a control sample. At the same time, the same amount of aptamer-conjugated AgNP solutions was added to 900 µl of PBS buffer with different *E.coli* concentrations. The concentrations used were 0 CFU/ml, 15×10^5 CFU/ml, 30×10^5 CFU/ml, 45×10^5 CFU/ml, 60×10^5 CFU/ml, 75×10^5 CFU/ml, 90×10^5 CFU/ml, and 105×10^5 CFU/ml. The mixtures were kept at room temperature for 15 min before recording absorbance spectra by a UV–visible spectrophotometer for 200–700 nm wavelengths.

Electrode modification and characterization

The SPCE was modified by drop-casting an AgNPs solution of 5 µl onto the working electrode surface and drying at 50 °C for 30 min (Perez-Rafols et al. 2017). After modification of the SPCE, CV was performed at a scan rate of 100 mV/s in the range -0.4 to + 0.4 for 10 cycles to strip out the loosely attached AgNPs and then washed with DI water for SEM analysis. Afterward, 5 µl of 5 µM aptamer solution was dispensed onto the working electrode and kept for drying at 4 °C for 24 h. Then, AgNPs and aptamer-modified SPCEs were washed three times using 200 µl of PBS buffer. Finally, 5 µl of 0.1 mM 2-mercaptoethanol was added to the modified electrodes and dried at room temperature to block the space and prevent the nonspecific binding of bacteria on the electrode. Figure 1 schematically shows the process steps for SPCE surface modification. Scanning electron microscopy (SEM) and energy dispersive spectroscopy (EDS) were performed to verify the presence of AgNPs on the SPCE surface.

A portable Potentiostat Emstat3® (Palmsens) was used to conduct the electrochemical analysis. CV on the bare SPCE and modified SPCE was performed at − 1.0 to 1.0 V and a scan rate of 100 mV/s using PBS buffer with 2.5 mM potassium ferricyanide and potassium ferrocyanide.

Time optimisation for aptamer-*E. coli* binding

The *E. coli* swim randomly in different directions and do not immediately appear on the sensing surface. The *E. coli* binding time was optimized by incubating a fixed concentration

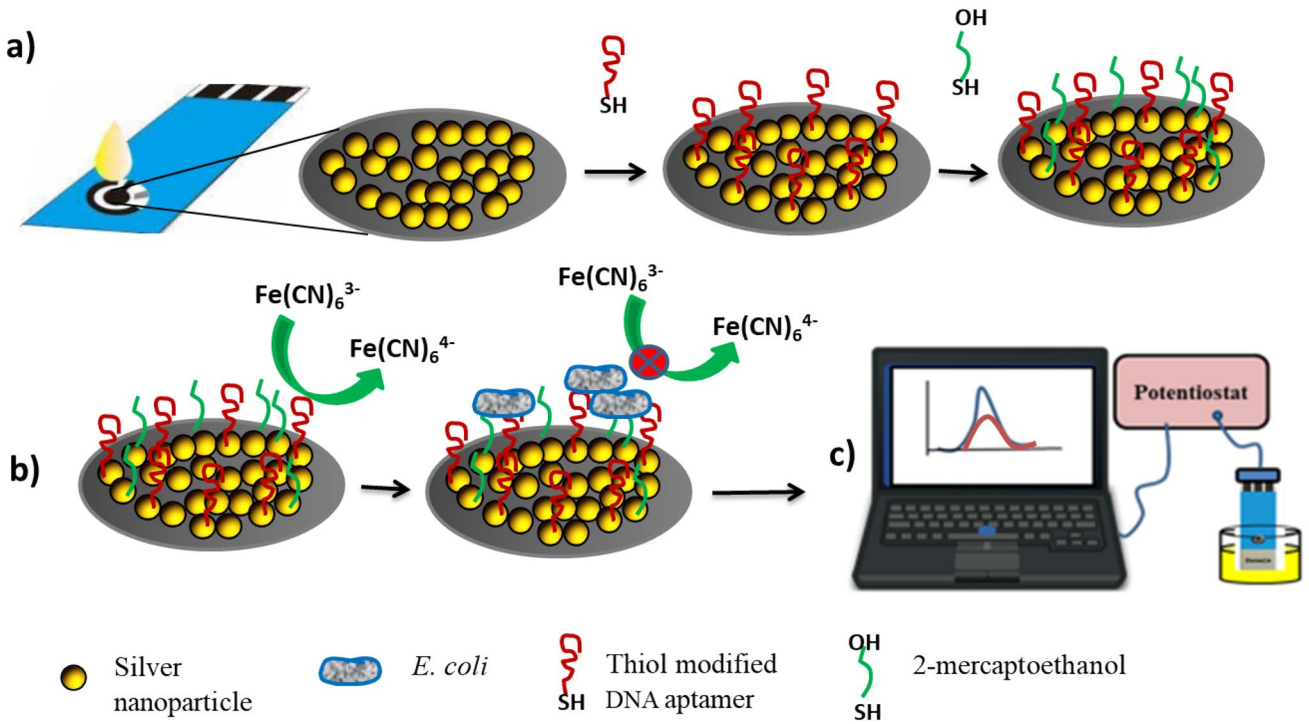

Fig.1 **a** Schematic illustration shows process steps of SPCE surface modifications that include drop-casting of the silver nanoparticles, attachment of thiol-modified aptamers, and blocking exposed areas of nanoparticles by 2-mercaptoethanol. **b** Potassium ferrocyanide and ferricyanide redox reagents were added to the solution just before the detection of E. coli, and **c** an experimental setup for the detection of bacteria using SPCE

of *E. coli* (15×10^2 CFU/ml) on the aptamer-modified SPCE for 5, 10, 15, and 20 min. After that, the differential pulse voltammetry (DPV) signals of *E. coli*-bound SPCE were recorded by a potentiostat for − 1 to 1 V at a pulse of 0.02 V for 0.02 s and a scan rate of 0.025 V/s.

Electrochemical analysis for *E. coli* detection

The DPV signals of aptamer and AgNP-modified SPCEs were recorded in an electrochemical cell containing various concentrations of *E.coli* in PBS buffer and 2.5 mM potassium ferricyanide and potassium ferrocyanide. DPV signals were measured at − 1 to 1 V, at a pulse voltage of 0.02 V for 0.02 s, and a scan rate of 0.025 V/s. The detection efficiency and limit of detection of modified SPCE were determined by measuring the DPV signal at *E. coli* concentrations of 150 CFU/ml, 15×10^2 CFU/ml, 15×10^3 CFU/ml, 15×10^4 CFU/ml, 15×10^5 CFU/ml, and 15×10^6 CFU/ml. The peak current was recorded from the DPV plot. All the experiments were carried out in duplicate. The current change concerning the log of *E. coli* concentration was plotted to get the regression curve.

Results and discussion

Silver nanoparticle characterization

AgNPs were synthesized by the chemical reduction method, in which sodium borohydride reduces the silver nitrate in the presence of the colloidal stabilizer polyvinylpyrrolidone (PVP). In this reaction, excess sodium borohydride (3 mM instead of 2 mM) was used to stabilize and increase the longevity of the AgNP colloid (Divsar et al. 2015). TEM images in Fig. 2a, b reveal that AgNPs are spherical and have a size distribution of 6.28 nm to 16.27 nm.

Figure 3a shows the DLS estimated hydrodynamic diameter and polydispersion index (PDI) of AgNPs dispersed in distilled water are about 41.84 nm (84.3% intensity) and 0.175, respectively. The large particle size in the DLS study might be due to the aggregation of particles in distilled water. PDI is a measure of the heterogeneity of the nanoparticle size. International Standards Organizations (ISOs) have established that PDI values less than 0.05 are more common in monodispersed samples. In contrast, PDI values greater than 0.7 indicate the polydisperse distribution of particles (Mudalige et al. 2019). Therefore, the AgNP colloid is considered a monodispersed sample according to the obtained PDI value. Zeta potential is the electrical potential at the slipping plane, which is the interface between the mobile fluid and the fluid attached to the nanoparticle surface. A high zeta potential ($> \pm 30$ mV) ensures good dispersibility and colloidal stability of nanoparticles in the liquid, as enough repulsive force prevents aggregation of the particles (Shnoudeh et al. 2019). The mean zeta potential of synthesized AgNPs was obtained at − 24.7 mV. The highest intense peak of the zeta potential was observed at − 31.9 mV, confirming the good colloidal stability of the particles (Fig. 3b).

Figure 3c, d show the size distribution profiles of AgNPs and aptamer conjugated AgNPs in 10 mM PBS buffer, respectively. The salts of the PBS buffer disrupt the equilibrium between electrostatic repulsion and break the stability of AgNPs, which causes the aggregation of nanoparticles and an increase in particle size (Christau et al. 2017).

Silver nanoparticle-aptamer conjugation

Metals such as gold (Au), silver (Ag), copper (Cu), and iron (Fe) are known to possess an affinity for sulfur (Hultberg et al. 1997). However, Cu nanoparticles are prone to instability in an open environment and tend to oxidize into CuO, resulting in reduced conductivity and stability (Yabuki and Tanaka 2011, Ma et al. 2022). Consequently, synthesizing Cu nanoparticles requires an inert gas system, making it challenging. Furthermore, the conjugation of thiol-modified aptamers on metal nanoparticles is a time-consuming

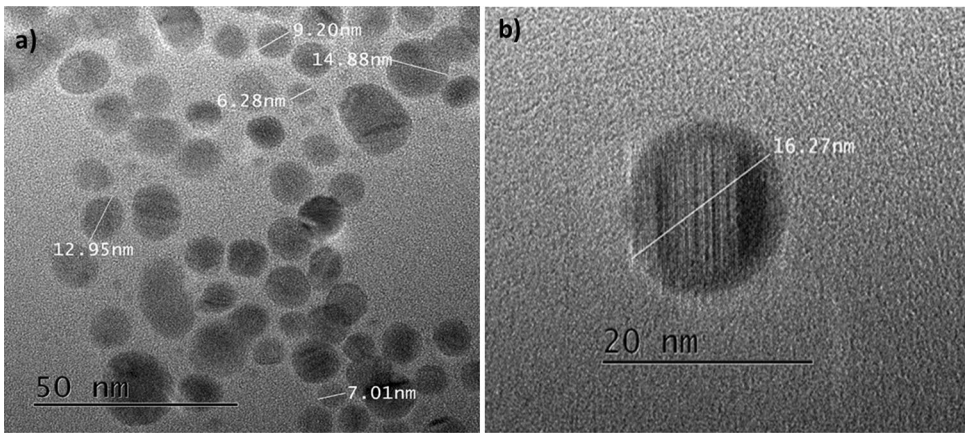

Fig. 2 **a** TEM analysis of spherical silver nanoparticles synthesized by the chemical reduction method. The size distribution shows that the diameters of nanoparticles are in the range of 6–17 nm, and (**b**) a high-resolution TEM image of a single silver nanoparticle

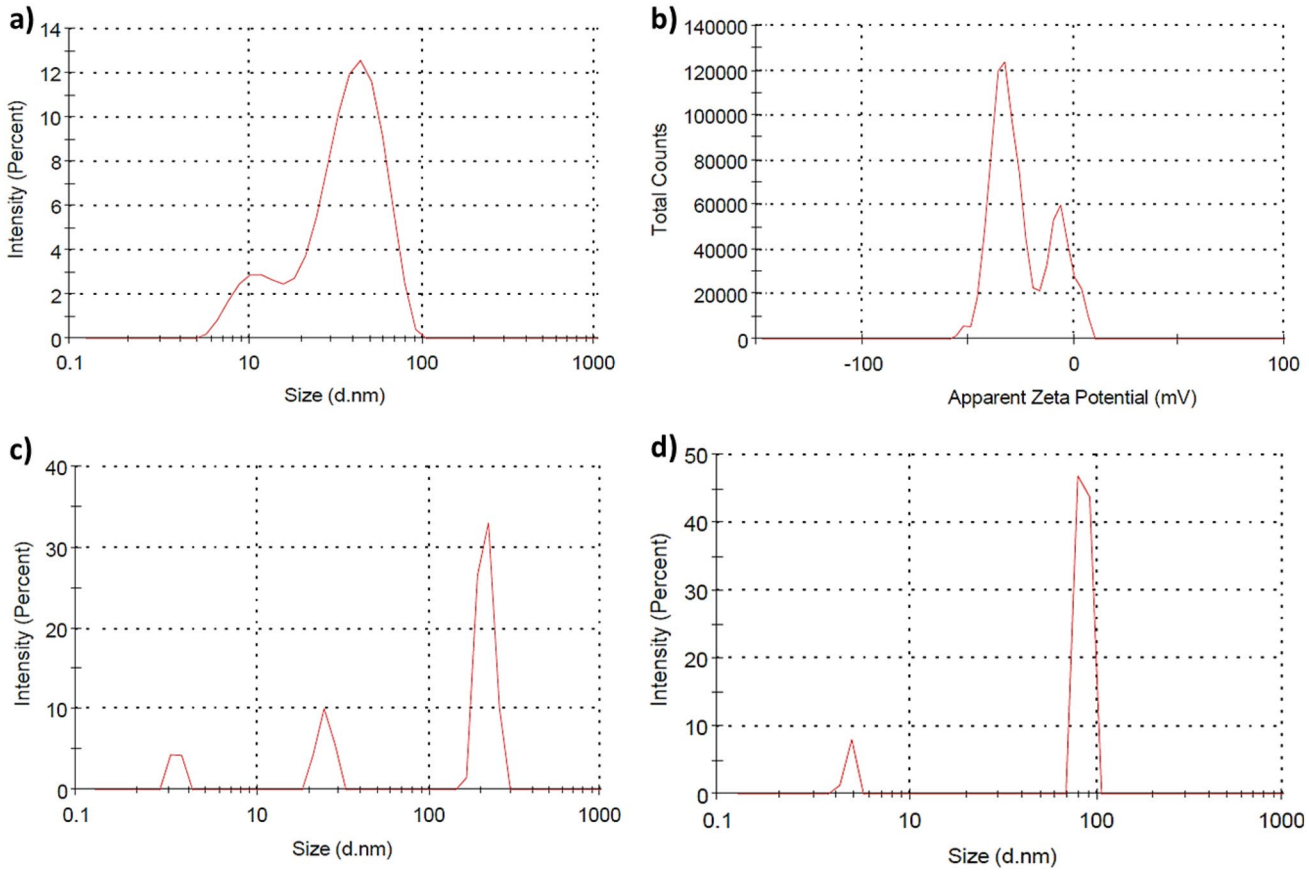

Fig. 3 **a** Size distribution profile of silver nanoparticles (AgNPs) in distilled water; **b** Zeta potential distribution of AgNPs in distilled water with size distribution profiles of **c** AgNPs in 10 mM PBS pH 7.4; and **d** aptamer conjugated AgNPs in 10 mM PBS pH 7.4

process that requires up to 24 h. This long exposure of Cu nanoparticles in buffer solution causes surface oxidation, hindering the formation of the Cu–S bonds. Similarly, pure Fe nanoparticles are not preferred due to their high tendency to oxidize quickly (Kelgenbaeva et al. 2014). There is no mention of direct thiol conjugation on iron oxide (Fe_3O_4) nanoparticles in the literature, as the presence of oxygen may block the interaction between Fe and S. Also, these nanoparticles get agglomerated in chain-like structures very easily (Xu et al. 2022). Even though the noble Au nanoparticles conjugate with thiol-modified aptamers, high material cost limits their large-scale applications. Ag nanoparticles provide advantages over other nanoparticles and are; therefore, they were selected for the conjugation with thiol (-SH) modified aptamers. The aptamer was thiol modified at the 5' end using C6 S–S phosphoramidite. The thiol groups are strong nucleophiles; thereby, unprotected thiol groups spontaneously form disulfides and dimers of aptamers, rendering the aptamers useless. The thiol groups were protected using disulfide phosphoramidite during the aptamer modification to avoid the formation of aptamer dimers.

Before the conjugation of aptamers with Ag, a potent reducing agent, TCEP was used as a reducing agent for aptamers to break the S–S bonds and form the -SH group. A high affinity of sulfur toward noble metals helps in the conjugation of the thiol-modified aptamer with silver through chemisorption or covalent bond formation (Yu and Li 2019; Zienkiewicz-Strzalka et al. 2018). AgNPs can be effectively functionalized with DNA molecules through a strong Ag–S bond. A short heating period of about 5 min is required before reduction to get the aptamer refolded in its proper 3-dimensional conformation. The addition of divalent cations like Mg^{2+} is essential to maintaining the looped structure of the aptamer (Hetzke et al. 2019). The incubation period and the size of AgNPs influence the process of aptamer-AgNP conjugation. Lower-size nanoparticles provide a high surface-to-volume ratio, essential for an influential and significant number of molecules binding (Rahnama et al. 2021).

The conjugation of thiol-modified aptamers with AgNPs was confirmed by studying the UV–visible absorption spectra of AgNPs, aptamers, and aptamer-conjugated AgNPs**.** Based on surface plasmon resonance (SPR) properties,

PVP-capped AgNPs showed a characteristic UV–visible absorbance peak at around 397 nm, and aptamer (DNA) shows an absorbance peak at about 260 nm, as shown in Fig. 4 (Derayeaa et al. 2017). At the same time, the conjugated nanoparticles show both absorbance peaks and confirm the successful conjugation of aptamer and nanoparticle (Fig. 4).

Additionally, CD spectroscopy analysis of aptamers, unmodified AgNPs, and aptamer conjugated AgNPs over the wavelength of 200 to 300 nm was used to observe structural changes of the aptamer upon target binding. Figure 5 shows no optical chirality for the unmodified AgNPs, whereas a strong optical chirality is observed for the aptamer in the UV region. The nonconjugated aptamers show a negative peak at around 250 nm and a positive peak at around 280 nm, identifying the aptamer's stem-loop (hairpin) structure (Yoshitomi et al. 2020; Zheng et al. 2011). Since the CD signals of aptamer-conjugated AgNPs show no shift in the peak positions, this study confirms no structural reassembling of the aptamer after conjugation with nanoparticles (Prante et al. 2019). A decrement in the positive and negative troughs in the CD signals for aptamer-conjugated AgNPs is due to the interaction of the aptamer molecules with Ag colloid and thus confirms the conjugation of the aptamer onto AgNPs (Kurt et al. 2016).

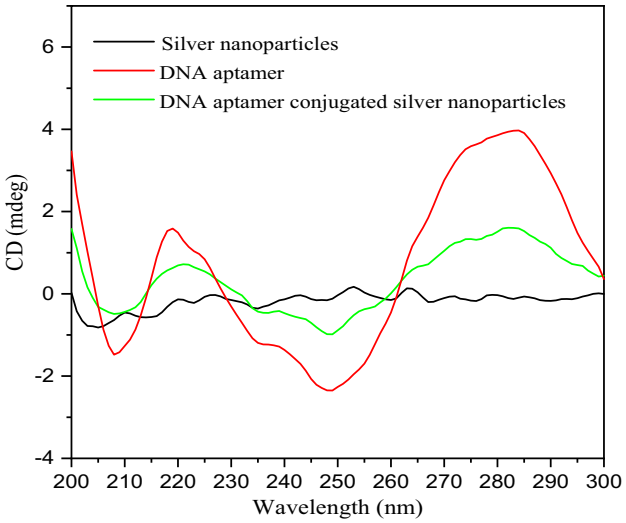

Fig. 5 Circular dichroism spectra of silver nanoparticles (AgNPs), free aptamer (1 µM), and aptamer conjugated to AgNPs (1 ml AgNPs treated with 1 µM of aptamer concentration). Each experiment was conducted in DI water with a sample volume of 500 µl. A decrement in the peak intensities confirms the bioconjugation of the AgNPs with aptamers

Affinity of the aptamer towards *E. coli* DH5α

The selected aptamers have a nearly similar extent of affinity towards most of the *E. coli* strains and a minimum binding affinity towards bacteria other than *E. coli* (Kim et al. 2013). The author did not analyze the binding affinity of the aptamer towards the *E. coli* DH5α strain. Therefore, UV–visible spectrophotometry was used to understand binding affinity and confirm the attachment of the aptamer to the *E. coli* DH5α strain in the study.

An increase in the ionic strength or addition of salt causes aggregation of nanoparticles exhibiting the change in the SPR region (Mavani and Shah 2013); therefore, the addition of AgNPs in PBS buffer significantly reduces the absorbance peak intensity. The particle size distribution of AgNPs before and after aptamer conjugation in DW and PBS was studied by DLS as presented in Fig. 3a, c, d, and the peak values are summarized in Table 1. Increased size and low zeta potential of AgNPs indicate aggregation of the nanoparticles in PBS buffer (Table 1, Fig. 3c). The increase in particle size and PDI index of AgNPs on conjugation with aptamers is probably due to the effects of salts present in PBS. However, this aggregation is not observed as irreversible.

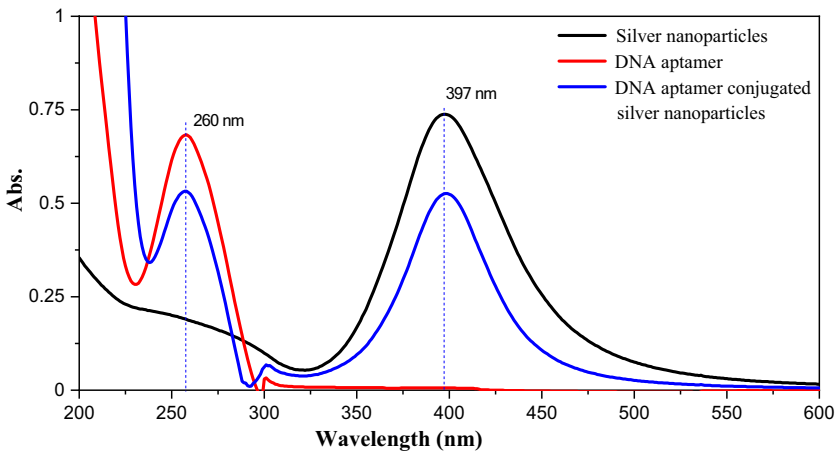

Fig.4 UV–visible spectra of aptamer-conjugated silver nanoparticles (AgNPs) compared with those of unconjugated AgNPs and free aptamers. The bioconjugation of AgNPs with aptamers is confirmed by the absorption peaks at 260 nm (for DNA) and 397 nm (for AgNPs). Experiments were conducted using 1 ml of each sample

Table 1 DLS particle size distribution and zeta potential of AgNP in DW and PBS

Composition	Particle size distribution (d.nm)	PDI	Zeta potential
AgNP in DW	Peak 1: 41.84 nm (84.3%) Peak 2: 11.08 nm (15.7%)	0.175	− 24.7
AgNP in PBS	Peak 1: 212 nm (71.3%) Peak 2: 24.72 nm (20.1%) Peak 3: 3.36 nm (8.7%)	1.00	− 6.85
AgNP-Aptamer in PBS	Peak 1: 84.84 nm (90.6%) Peak 2: 4.755 nm (9.4%)	1.00	− 9.32

The aptamers have a high affinity for *E. coli*; thus, incubation of aggregated AgNPs with the bacterial suspension causes redispersion of the conjugated AgNPs in the solution. The absorbance peak of UV–visible spectrophotometry was significantly increased on incubation of aptamer-AgNPs with *E. coli,* which resulted in the binding of AgNP-aptamer on the *E. coli* cells and redispersion in PBS buffer (Fig. 6). A similar observation has been reported by Sepunaru et al. (2015)**,** who described the change in SPR and increased absorbance peak intensity of AgNPs on binding with *E. coli*. The absorbance peak value increases linearly with increasing *E. coli* concentrations. The equation of the linear regression curve $Y = 0.0002X + 0.0103$ is obtained with an R^2 value of 0.96, indicating a good agreement of experimental results of UV–visible spectrophotometry with analytical performance. The redispersion phenomena of aptamer-AgNPs and the above correlation of absorbance with concentration propose that aptamer has a high affinity for *E. coli*.

Electrode modification and electrochemical analysis

The SPCE used in the current work is a miniature version of the conventional electrodes. The drop-casted AgNPs serve as an immobilization platform for thiol-modified aptamers and electron transporters. Aptamers modified with a thiol (-SH) group at the terminal nucleotide were conjugated to the silver nanoparticles as the sulfur has a strong affinity for noble metals like silver (Labib et al. 2012). Aptamers are single-stranded nucleic acids that act as recognition elements and selectively bind to the targeted *E. coli*.

Electrode characterization

The characterization of the modified electrode is essential for understanding the degree of functionalization, redox reactions, and uniformity in modifications, which are essential to carrying out errorless sensing experiments. After cleaning the AgNp-modified SPCE, SEM analysis and EDS mapping were carried out to confirm the presence of AgNPs on

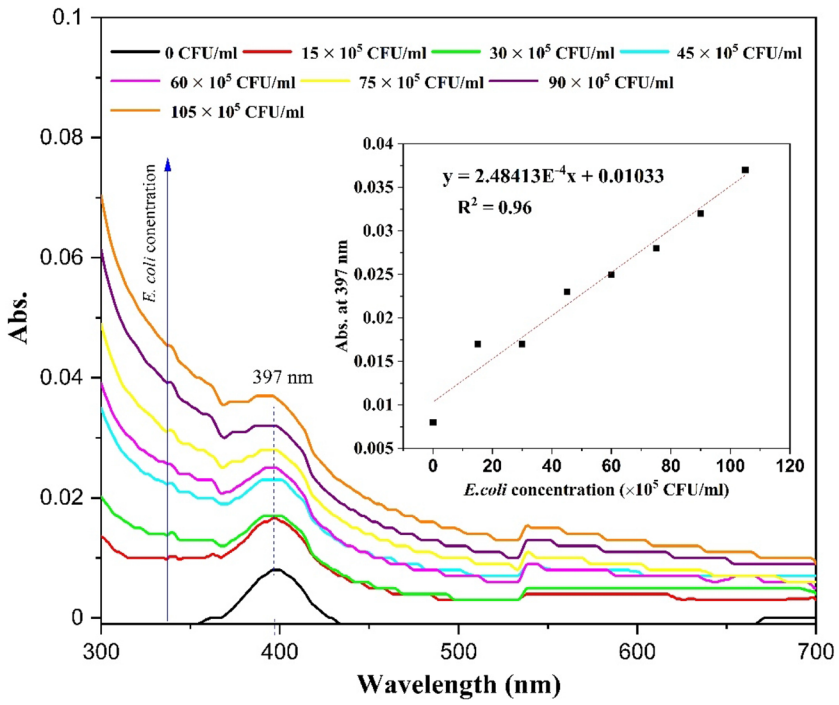

Fig. 6 UV–visible spectrophotometric analysis of the aptamer-conjugated AgNPs with increasing E. coli concentrations. The linear increment in the absorption concerning the E. coli concentrations is shown in the inset. Each experiment was done in 10 mM PBS, pH 7.4, and a sample volume of 1 ml

the electrode surface, which will eventually prove the firm attachment of the AgNPs to the electrode surface. The SEM micrograph (Fig. 7a) shows the homogeneous distribution of the fine nanoparticles all over the electrode surface**.** EDS mapping represents carbon (C K) in green and silver (Ag L) in red in Fig. 7b, c, respectively**.** Figure 7d represents the distribution of Ag over C, and the graphical EDS data presented in Fig. 7e showing the respective peaks for Ag confirms the presence of AgNPs on the electrode surface.

A cyclic voltammetry analysis confirms the aptamer binding onto the electrode surface by analyzing the redox reaction occurring at the electrode–electrolyte interface. The redox reaction mediated by potassium ferrocyanide and potassium ferricyanide as redox species is presented in Eq. 2.

$$Fe(CN)_6^{3-} + e^- \underset{\text{Oxidation}}{\overset{\text{Reduction}}{\rightleftharpoons}} Fe(CN)_6^{4-} \quad (2)$$

AgNPs have high surface free energy due to their high surface-to-volume ratio, which causes signal amplification. Therefore, AgNPs drop-casted SPCE electrode shows an increase in peak current intensity of the oxidation and reduction peaks due to the enhancement of conductivity of the electrode. Also, AgNPs are very compatible with biomolecules. On immobilizing the aptamer on the electrode, a decline in peak current occurred due to the electrostatic repulsion between the negatively charged aptamer (DNA) and the ferrocyanide-ferricyanide species (Ma et al. 2014). The sequential decline in anodic current peak (Ip_a) and cathodic current peak (Ip_c) after the addition of aptamer indicates successful functionalization of the aptamer on the

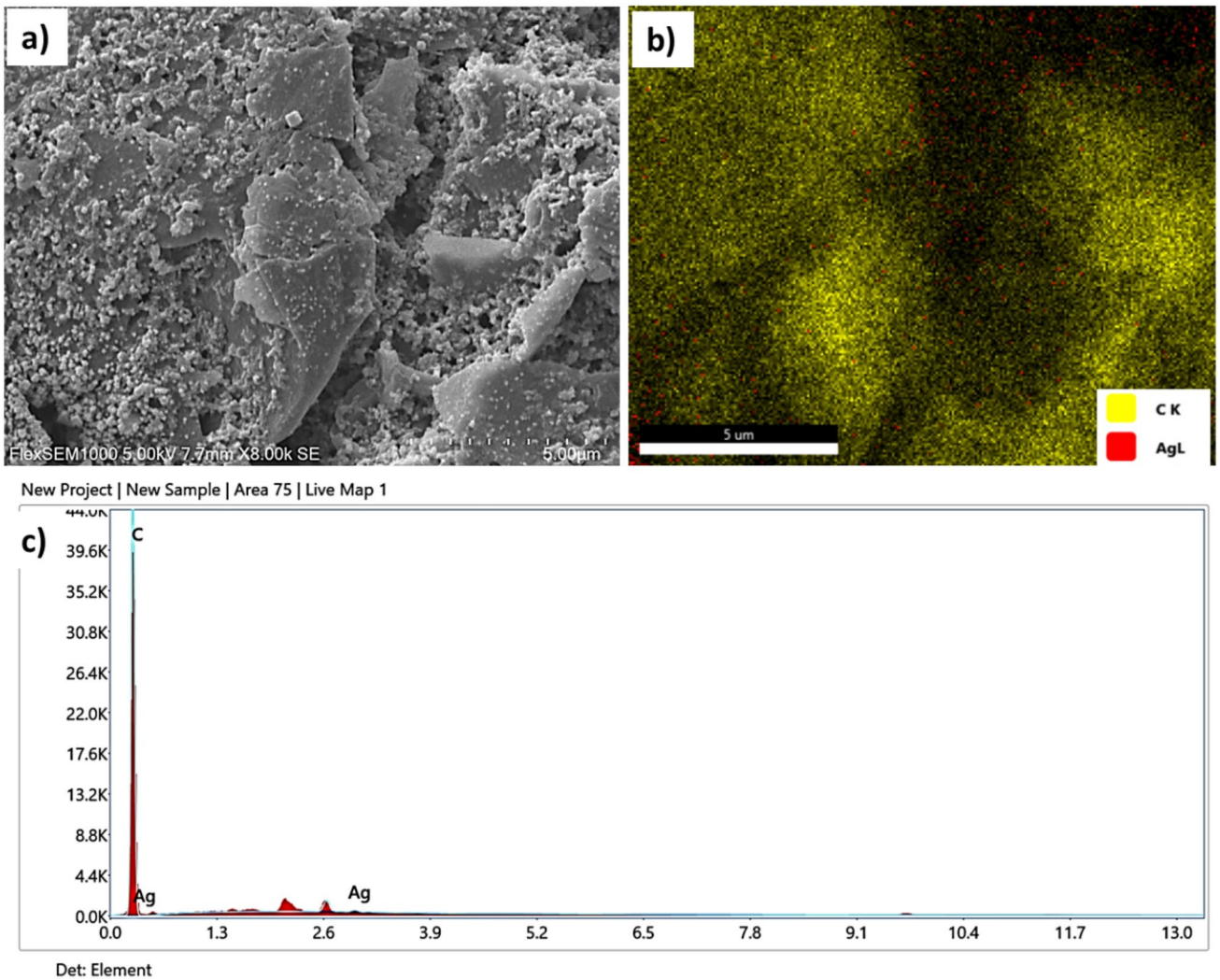

Fig. 7 **a** SEM micrograph of SPCE decorated with drop-casted AgNPs. EDS mapping of AgNP modified SPCE showing C K, and Ag L, **c** EDS graph showing peaks of C and Ag elements

electrode surfaces (Labib et al. 2012). The redox peak current and intensities decrease significantly as the aptamers cover a large electrode area (Fig. 8). Further, the deposition of 2-mercaptoethanol covers the electrode active surface area, causing resistance to the charge transfer at the electrode surface. CV analysis of bare SPCE and modified electrodes shows an anodic peak (oxidation) at around + 0.45 V and a cathodic peak (reduction) at around − 0.19 V, as shown in Fig. 8.

A considerable amount of aptamer can remain loosely bound to the electrode surface and disperse into the solution during electrochemical experiments. Washing is essential to remove unbound aptamer molecules and avoid experimental errors. 2-mercaptoethanol has a thiol group, which has an affinity for AgNPs. Therefore, any exposed area of AgNPs after aptamer modification will be covered by 2-mercaptoethanol. This step is necessary to avoid nonspecific binding of *E. coli,* which may lead to technical errors during sensing experiments.

Optimisation of the incubation time

Although biorecognition agents like DNA aptamers are highly sensitive and specific, they require a particular time to interact and bind with the targets, as *E. coli* continuously swims and tumbles in random directions. In the electrochemical analysis and detection of the bacterial population in the water sample, it is necessary to find the optimum binding time through which a significant signal change can be obtained. DPV signals were recorded for variable periods at a fixed concentration of *E. coli* (15×10^2 CFU/ml). The current vs. time plot in Fig. 9 shows a significant decrease in the current signals until the incubation time of 15 min, and no substantial change in the current was observed after 15 min. The findings in the above study suggested that a binding time of 15 min is an optimum response time for the biosensor. Therefore, all the electrochemical analysis was carried out by incubating the aptamer-modified SPCE with *E. coli* dilutions for 15 min.

Biosensor calibration curve and selectivity

The change in electrochemical signal concerning the bacteria concentration was analyzed by differential pulse voltammetry (DPV), a voltammetric technique with enhanced discrimination of Faradic currents, i.e., electron transfer to and from the electrode. DPV is a highly sensitive method because of the minimization of the capacitive current or background charges (Simoes and Xavior 2017). DPV studies can provide improved selectivity for observing the differences in redox processes compared to CV studies. The experiments were conducted at various pulse voltages from 10 to 50 mV for 0.02 s at a 25 mV/s scan rate to optimize the pulse voltage and get recognizable signals. A pulse voltage of 20 mV was found ideal for efficient signal discrimination for bare and modified electrodes and at different analyte concentrations.

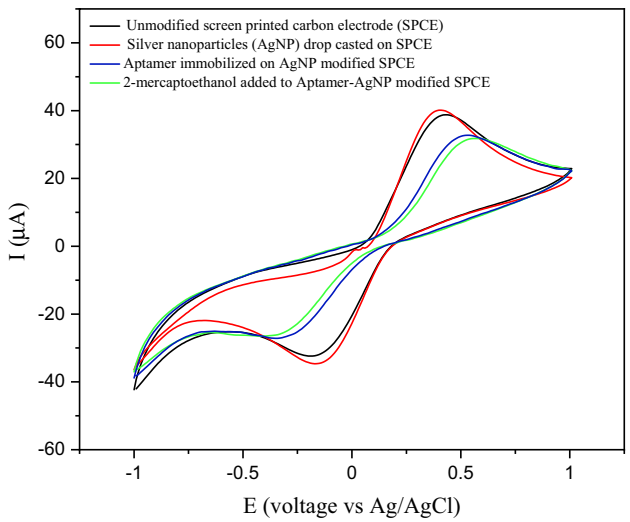

Fig. 8 Cyclic voltammetry analysis of each modification step, including bare unmodified SPCE, AgNP drop-casted SPCE (Ag-SPCE), aptamer-functionalized Ag-SPCE, and 2-mercaptoethanol blocking the unbound sites on the aptamer-functionalized Ag-SPCE sensor. The electrode modifications were confirmed as AgNP drop casting increases the redox peak intensity, whereas aptamer functionalization reduces the redox peak intensity. Experimental conditions: Each experiment was performed using 5 ml of 10 mM PBS pH 7.4 containing 2.5 mM $Fe(CN)_6^{3-/4-}$

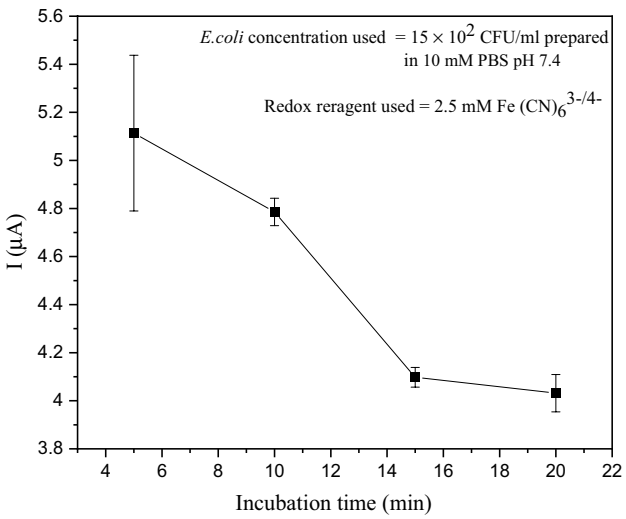

Fig. 9 Plot of current (I) vs. incubation time for optimizing the response time. The current response does not decrease significantly after 15 min, considered an optimum incubation time for aptamer-E. coli binding on the electrode surface

Finally, the detection of *E. coli* was performed by AgNPs and aptamer-modified SPCE at optimized response time and pulse voltage. The DPV results show a decrease in peak current with an increase in *E. coli* concentration (Fig. 10a, b) due to the blockage of electron transfer by aptamer-captured bacterial cells. The bacteria attached to the electrode surface cause resistance to the charge transfer from the electrode to the $Fe(CN)_6^{3-/4-}$. As a result, the increase in bacterial concentration in the solution increases the number of bacterial attachments on the sensor surfaces and decreases the current intensity. The current change is attributed as ΔI and plotted against the log of *E.coli* concentration to get a regression line expression, illustrated in Fig. 10b and presented in Eq. 3.

$$\Delta I = 0.2934\,X + 0.838 \quad (3)$$

$$C = \text{Antilog } X \quad (4)$$

Equation 3 denotes that the change in current (ΔI) across the sensor is directly proportional to the log of *E. coli* concentration (X). A high R^2 value of 0.98 supports the conclusion that the correlation between the current signal and the logarithmic value of the *E. coli* concentration can be utilized to quantify the presence of bacteria in the water sample. The actual *E. coli* concentration (C) in CFU/ml can be determined by calculating the antilog of X, as represented in Eq. 4. To analyze the selectivity, DPV was carried out on the 15,000 CFU/ml concentration of three different bacterial strains, viz., *Serratia marcescens*, *Bacillus subtilis*, and *Staphylococcus aureus,* in PBS pH 7.4, using the developed biosensor, and the signals obtained were compared with the same concentration of *E. coli*. Figure 11 shows that all three bacterial strains other than E. coli show very little intensity of the current change (ΔI) compared to that of *E. coli,* proving the excellent selectivity of the proposed biosensor.

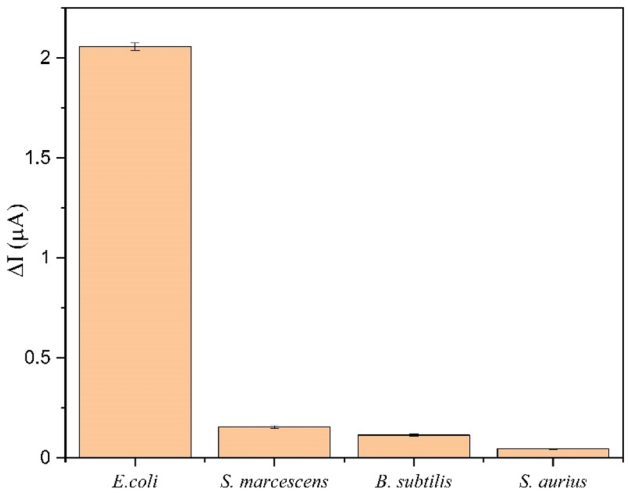

Fig. 11 Current change (ΔI) data from DPV analysis of the three different bacterial strains obtained individually and compared with E. coli. Experimental conditions: 15,000 CFU/ml of concentration of each strain prepared in 10 mM PBS, pH 7.4

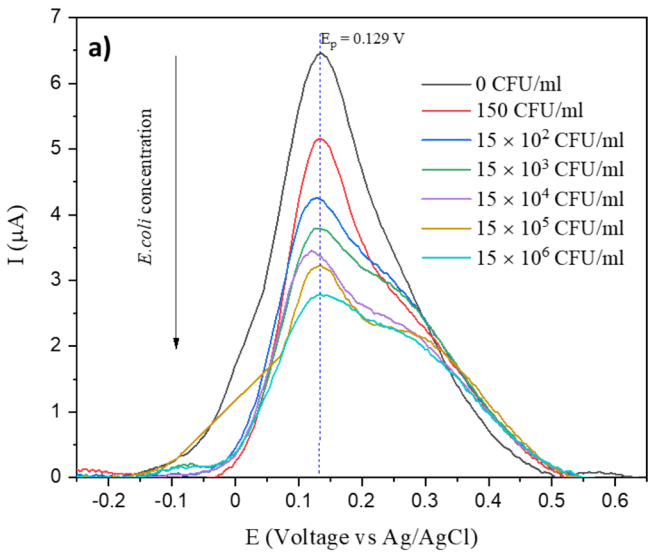

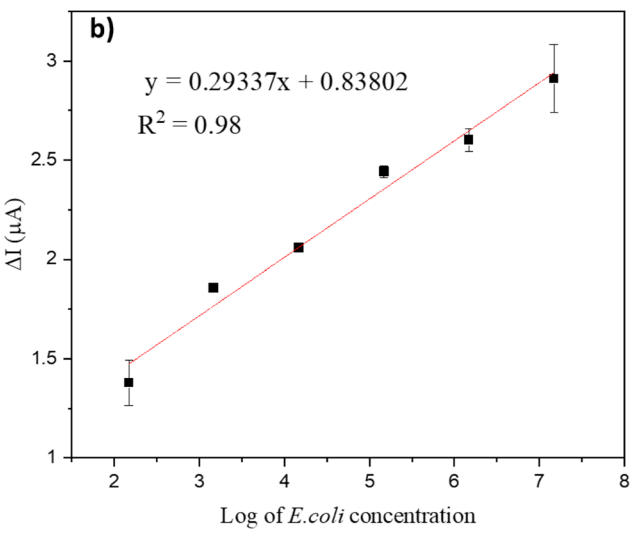

Fig. 10 **a** DPV measurements in the presence of increasing E. coli concentrations. **b** Regression curve for E. coli detection plotted as current change (ΔI) vs. log of concentration. Experimental conditions: Each experiment was performed using 5 ml of coli concentration prepared in 10 mM PBS pH 7.4 containing 2.5 mM $Fe(CN)_6^{3-/4-}$ as a redox reagent. The E. coli concentrations used are 150 CFU/ml, 15×10^2 CFU/ml, 15×10^3 CFU/ml, 15×10^4 CFU/ml, 15×10^5 CFU/ml, and 15×10^6 CFU/ml

Table 2 Validation of the biosensor with *E. coli* spiked water samples

Known concentration	Detected concentration	% Recovery	% Error
200 CFU/ml	190.54 CFU/ml	95.27	− 4.73
2000 CFU/ml	1949.84 CFU/ml	97.49	− 2.51
60,000 CFU/ml	64,565.42 CFU/ml	107	+ 7

RSD, LOD, and validation and stability of biosensor

Reproducibility is an essential parameter for a new method, evaluated by the relative standard deviation (RSD) value. The measurements of DPV current signals at each concentration of *E. coli* were replicated three times. The RSD values of three replicates at 150 CFU/ml, 15×10^2 CFU/ml, and 15×10^3 CFU/ml were obtained as 6.91%, 2.75%, and 1.47%, respectively, which show good reproducibility of results. The higher deviation is observed at lower concentrations, as the attachment of a sufficient number of bacteria to cause a noticeable current change is challenging. The *E. coli* concentration of 150 CFU/ml was found to be the limit of detection (LOD) and the limit of quantification (LOQ) for the proposed biosensor. Brosel-oliu et al. (2018) demonstrated an impedimetric aptamer sensor for detecting *E. coli* O157:H7 with a LOD of 100 CFU/ml. The authors used the vapor phase silanization method to modify the tantalum silicide electrode with 3-mercaptopropyltrimethoxysilane for binding the thiol-modified aptamer. Queiros et al. (2013) fabricated an aptamer-based impedimetric biosensor by immobilizing a thiol-modified aptamer on a gold electrode surface to detect *E. coli* outer membrane proteins. A DNA probe-based electrochemical biosensor was developed by Xu et al. (2017) for the detection of *E. coli* O157 genomic DNA. The author immobilized the captured DNA onto a graphene oxide-chitosan-modified glassy carbon electrode using EDC-NHS linker molecules. These biosensors are designed for repetitive use; however, their functionality reduces over time and requires the pretreatment of the samples. A reduced graphene oxide-based field effect transistor sensor was developed by Saha et al. (2018) using aptamer-conjugated magnetic nanoparticles to detect *E. coli* in aqueous samples. The author mentioned aptamer functionalization of the nanoparticles using EDC-NHS coupling and about an hour of incubation time for aptamer-*E. coli* binding. Vu et al. (2021) have reported the electrochemical detection of *E. coli* O157 by immobilizing antibodies onto gold nanoparticles via EDC-NHS linkage. However, the antibodies have some limitations: they are expensive, difficult to synthesize, thermally sensitive, and unstable compared to the aptamer. Dinshaw et al. (2017) demonstrated a highly sensitive electrochemical aptasensor for detecting *Salmonella* with a LOD of 10 CFU/ml by using a reduced graphene oxide-chitosan composite as an immobilization platform. The thiol-modified aptamers were functionalized on the electrode through glutaraldehyde crosslinking with amino groups of chitosan. Their methodology of sensor fabrication is the most complicated and time-consuming, and it requires linking molecules like EDC-NHS. The biosensor fabrication method proposed in the current study directly immobilizes the aptamer on the AgNPs, requires no linker molecules, and provides high sensitivity in a short incubation time.

Further, the applicability of the aptamer-AgNPs-modified bacterial sensors was verified using tap water samples spiked with known concentrations of *E. coli*. The pH of the sample medium was neutral (7.2). Potassium ferrocyanide and ferricyanide redox reagents of 2.5 mM concentration (molar ratio 1:1) were added to the sample before recording the DPV response. The percentage recovery and error were calculated using Eq. 5 and Eq. 6, respectively.

$$\%\ \text{Error} = \frac{(\textit{known concentration} - \textit{detected concentration})}{\textit{known concentration}} \times 100 \quad (5)$$

$$\%\ \text{Recovery} = 100 - \%\ \text{Error} \quad (6)$$

The analysis presented in Table 2 shows that sensors have recoveries ranging from 95.27% to 107%, indicating satisfactory accuracy of the proposed biosensor for detecting bacteria. The stability of the biosensor was assayed using the LOD concentration of 150 CFU/ml for four weeks at room temperature. The biosensor was found to be stable, as the ΔI signals shown in Table 3 were within the range of the standard deviation.

Conclusions

The study illustrates the use of silver nanoparticles as a functionalization platform for aptamer-based sensor development. The bioconjugation of silver nanoparticles with aptamers can be successfully implemented in electrochemical biosensing applications to detect bacteria. Silver nanoparticles were used as an effective platform for immobilizing bacteria-specific aptamers while modifying screen-printed electrodes. Silver nanoparticles were used as an effective

Table 3 Stability of the biosensor

DPV for 150 CFU/ml ΔI (average ± SD)	1st week	2nd week	3rd week	4th week
1.37927 ± 0.112415 µA	1.436625 µA	1.437325 µA	1.376615 µA	1.370155 µA

platform for immobilizing bacteria-specific aptamers while modifying screen-printed electrodes. The screen-printed carbon electrodes are used to develop advanced biosensors, which are miniaturized three-electrode systems, compact in design and portable to remote areas. These biosensors are ideal for onsite detection of the bacteria in real-time as they exhibit a response time of about 15 min and do not require pretreatment, sophisticated lab facilities, and skilled personnel. Detecting bacteria in tap water demonstrated a proof of concept for rapid, selective, and easy onsite detection. The prepared biosensors exhibit high sensitivity, with a LOD of 150 CFU/ml. The biosensor demonstrated a pronounced selectivity for *E.coli* compared to the response signals obtained from other bacteria. The biosensors displayed good reproducibility, as indicated by a relative standard deviation (RSD) of 6.91% (n = 3). Moreover, the biosensor remained stable at room temperature for four weeks and exhibited excellent recovery rates ranging from 95.27% to 107% during the tap water sensitivity validation. The screen-printed electrodes are comparatively cheaper than conventional electrodes but cannot be used repeatedly, thus decreasing the cost per assay. Also, there is an advantage concerning the loss of functionality over time due to the repeated use of conventional electrodes. Moreover, SPCEs make the device compact and favorable for transport. High reproducibility, sensitivity, recoveries from spiked samples, and a lower limit of detection make developed biosensors reliable and robust sensors for practical application.

Acknowledgements This research was supported by the Science and Engineering Research Board (SERB), India (EEQ/2018/000509) and National Mission on Himalayan Study (NMHS) (NMHS/2022-23/SG 82/02/285).

Author contributions AHD: design and conception, original drafting of the article, data curation; RPV: methodology and editing; BP: facilitating microbiological aspects; AK: facilitating characterization; BS: conceptualization, supervision, guidance on characterization, writing, reviewing, and editing.

Funding The Science and Engineering Research Board, India (EEQ/2018/000509) and National Mission on Himalayan Study (NMHS) (NMHS/2022-23/SG 82/02/285) funded the work.

Declarations

Conflict of interest The authors declare no conflict of interest to disclose.

Consent for publication This work does not involve human participants or animals and also does not include any person's data in any form, so no permission is needed.

References

Altintas Z, Akgun M, Kokturk G, Uludag Y (2018) A fully automated microfluidic-based electrochemical sensor for real-time bacteria detection. Biosens Bioelectron 100:541–548. https://doi.org/10.1016/j.bios.2017.09.046

Brosel-Oliu S, Ferreira R, Uria N, Abramova N, Gargallo R, Munoz-Pascual FX, Bratov A (2018) Novel impedimetric aptasensor for label-free detection of *Escherichia coli* O157: H7. Sens Actuators, B Chem 255:2988–2995. https://doi.org/10.1016/j.snb.2017.09.121

Bu S, Wang K, Li Z, Wang C, Hao Z, Liu W, Wan J (2020) An electrochemical biosensor based on methylene blue-loaded nanocomposites as signal-amplifying tags to detect pathogenic bacteria. Analyst 145:4328–4334. https://doi.org/10.1039/D0AN00470G

Christau S, Moeller T, Genzer J, Koehler R, von Klitzing R (2017) Salt-induced aggregation of negatively charged gold nanoparticles confined in a polymer brush matrix. Macromolecules 50:7333–7343. https://doi.org/10.1021/acs.macromol.7b00866

De A, Kalita D (2021) Bio-fabricated gold and silver nanoparticle based plasmonic sensors for detection of environmental pollutants: an overview. Critical Rev Analytical Chem. https://doi.org/10.1080/10408347.2021.1970507

Derayeaa SM, Omar MA, Hammad MA, Hassanb YF (2017) Application of surface plasmon resonance of citrate capped silver nanoparticles for the selective determination of some fluoroquinolone drugs. J Appl Pharma Sci 7:016–024. https://doi.org/10.7324/JAPS.2017.70203

Dinshaw IJ, Muniandy S, Teh SJ, Ibrahim F, Leo BF, Thong KL (2017) Development of an aptasensor using reduced graphene oxide chitosan complex to detect Salmonella. J Electroanal Chem 806:88–96. https://doi.org/10.1016/j.jelechem.2017.10.054

Divsar F, Habibzadeh K, Shariati S, Shahriarinour M (2015) Aptamer conjugated silver nanoparticles for the colorimetric detection of arsenic ions using response surface methodology. Anal Methods 7:4568–4576. https://doi.org/10.1039/c4ay02914c

Elmund GK, Allen MJ, Rice EW (1999) Comparison of *Escherichia coli*, total coliform, and fecal coliform populations as indicators of wastewater treatment efficiency. Water Environ Res 71:332–339. https://doi.org/10.2175/106143098X121752

Foddai AC, Grant IR (2020) Methods for detection of viable foodborne pathogens: current state-of-art and future prospects. Appl Microbiol Biotechnol 104:4281–4288. https://doi.org/10.1007/s00253-020-10542-x

Hetzke T, Vogel M, Gophane DB, Weigand JE, Suess B, Sigurdsson ST, Prisner TF (2019) Influence of Mg^{2+} on the conformational flexibility of a tetracycline aptamer. RNA 25:158–167. https://doi.org/10.1261/rna.068684.118

Housaindokht MR, Verdian A, Sheikhzadeh E, Pordeli P, Zaeri ZR, Fard FJ, Pour AN (2018) A sensitive electrochemical aptasensor based on single wall carbon nanotube modified screen-printed electrode for detection of Escherichia coli O157: H7. Adv Mater Lett 9:369–373. https://doi.org/10.5185/amlett.2018.1701

Hultberg B, Andersson A, Isaksson A (1997) Copper ions differ from other thiol-reactive metal ions in their effects on the concentration and redox status of thiols in HeLa cell cultures. Toxicology 117:89–97. https://doi.org/10.1016/s0300-483x(96)03554-8

Kaur H, Shorie M, Sabherwal P (2020) Electrochemical aptasensor using boron-carbon nanorods decorated by nickel nanoparticles for detection of E. coli O157: H7. Microchim Acta 187:1–10. https://doi.org/10.1007/s00604-020-04444-y

Kelgenbaeva Z, Omurzak E, Takebe S, Sulaimankulova S, Abdullaeva Z, Iwamoto C, Mashimo T (2014) Synthesis of pure

iron nanoparticles at liquid–liquid interface using pulsed plasma. J Nanopart Res 16:1–11. https://doi.org/10.1007/s11051-014-2603-z

Khan FM, Gupta R (2020) Escherichia coli (*E. coli*) as an Indicator of Fecal Contamination in Groundwater: A Review. In International Conference on Sustainable Development of Water and Environment, pp. 225–235. Springer, Cham.

Kim YS, Song MY, Jung J, Kim BC (2013) Isolation and characterization of DNA aptamers against Escherichia coli using a bacterial cell–systematic evolution of ligands by exponential enrichment approach. Anal Biochem 436:22–28. https://doi.org/10.1016/j.ab.2013.01.014

Kurt H, Yuce M, Hussain B, Budak H (2016) Dual-excitation upconverting nanoparticle and quantum dot aptasensor for multiplexed food pathogen detection. Biosens Bioelectron 81:280–286. https://doi.org/10.1016/j.bios.2016.03.005

Labib M, Zamay AS, Muharemagic D, Chechik A, Bell JC, Berezovski MV (2012) Electrochemical sensing of aptamer-facilitated virus immunoshielding. Anal Chem 84:1677–1686. https://doi.org/10.1021/ac202978r

Li Y, Schluesener HJ, Xu S (2010) Gold nanoparticle-based biosensors. Gold Bull 43:29–41. https://doi.org/10.1007/BF03214964

Ma X, Jiang Y, Jia F, Yu Y, Chen J, Wang Z (2014) An aptamer-based electrochemical biosensor for the detection of Salmonella. J Microbiol Methods 98:94–98. https://doi.org/10.1016/j.mimet.2014.01.003

Ma X, Zhou S, Xu X, Du Q (2022) Copper-containing nanoparticles: Mechanism of antimicrobial effect and application in dentistry-a narrative review. Frontiers in Surgery. https://doi.org/10.3389/surge.2022.905892

Mathelie-Guinlet M, Cohen-Bouhacina T, Gammoudi I, Martin A, Beven L, Delville MH, Grauby-Heywang C (2019) Silica nanoparticles-assisted electrochemical biosensor for the rapid, sensitive, and specific detection of Escherichia coli. Sens Actuators, B Chem 292:314–320. https://doi.org/10.1016/j.snb.2019.03.144

Mavani K, Shah M (2013) Synthesis of silver nanoparticles by using sodium borohydride as a reducing agent. Inter J Eng Res Tech 2:1–5. https://doi.org/10.1371/journal.pone.0057189

Mudalige T, Qu H, Van Haute D, Ansar SM, Paredes A, Ingle T (2019) Characterization of nanomaterials: Tools and challenges. Nanomaterials Food Applications. https://doi.org/10.1016/B978-0-12-814130-4.00011-7

Perez-Rafols C, Bastos-Arrieta J, Serrano N, Diaz-Cruz JM, Arino C, De Pablo J, Esteban M (2017) Ag nanoparticles drop-casting modification of screen-printed electrodes for the simultaneous voltammetric determination of Cu (II) and Pb (II). Sensors 17:1458. https://doi.org/10.3390/s17061458

Prante M, Schuling T, Roth B, Bremer K, Walter J (2019) Characterization of an Aptamer directed against 25-hydroxyvitamin D for the development of a competitive aptamer-based Assay. Biosensors 9:134. https://doi.org/10.3390/bios9040134

Queiros RB, de-Los-Santos-Alvarez N, et al. (2013) A label-free DNA aptamer-based impedance biosensor for the detection of *E. coli* outer membrane proteins. Sensors and Actuators B: Chemical, 181:766-772. doi:https://doi.org/10.1016/j.snb.2013.01.062

Rahnama S, Shariati S, Divsar F (2021) Selective aptamer conjugation to silver-coated magnetite nanoparticles for magnetic solid-phase extraction of trace amounts of Pb2+ ions. RSC Adv 11:4971. https://doi.org/10.1039/D1RA00006C

Sabouri S, Ghourchian H, Shourian M, Boutorabi M (2014) A gold nanoparticle-based immunosensor for the chemiluminescence detection of the hepatitis B surface antigen. Anal Method 6:5059–5066. https://doi.org/10.1039/c4ay00461b

Saha B, Purwar P, Lee J, Saha S (2018) Magnetic nanoparticle encapsulation for the manipulation of bacterial movement and spontaneous detection by reduced graphene oxide. Adv Biosyst 2:1800095. https://doi.org/10.1002/adbi.201800095

Sepunaru L, Tschulik K, Batchelor-McAuley C, Gavish R, Compton RG (2015) Electrochemical detection of single *E. coli* bacteria labeled with silver nanoparticles. Biomat Sci 3:816–820. https://doi.org/10.1039/C5BM00114E

Shen Q, Wang X, Chen E, Ma Z (2019) Comparative Study on Test Methods of Total Coliforms in Domestic Drinking Water. In IOP Conference Series: Earth and Environmental Science, pp 042002. IOP Publishing. doi:https://doi.org/10.1088/1755-1315/310/4/042002

Shnoudeh AJ, Hamad I, Abdo RW, Qadumii L, Jaber AY, Surchi HS, Alkelany SZ (2019) Synthesis, characterization, and applications of metal nanoparticles. In Biomaterials and Bionanotechnology, pp 527–612. Academic Press. doi:https://doi.org/10.1016/B978-0-12-814427-5.00015-9

Siller IG, Preuss JA, Urmann K, Hoffmann MR, Scheper T, Bahnemann J (2020) 3D-printed flow cells for aptamer-based impedimetric detection of E. coli crook's strain. Sensors. https://doi.org/10.3390/s20164421

Simoes FR, Xavior MG (2017) Electrochemical sensors. In Nanoscience and its applications, pp. 155-178. William Andrew Applied Science Publisher. Doi:https://doi.org/10.1021/ac0202278

Sugawa K, Tahara H, Yamashita A, Otsuki J, Sagara T, Harumoto T, Yanagida S (2015) Refractive index susceptibility of the plasmonic palladium nanoparticle: potential as the third plasmonic sensing material. ACS Nano 9:1895–1904. https://doi.org/10.1021/nn506800a

Templier V, Roux A, Roupioz Y, Livache T (2016) Ligands for label-free detection of whole bacteria on biosensors: a review. TrAC, Trends Anal Chem 79:71–79. https://doi.org/10.1016/j.trac.2015.10.015

U. S. Environmental protection agency, (1976) https://www.epa.gov/wqc/quality-criteria-water-red-book Accessed on 1 January 2023.

Vikesland PJ (2018) Nanosensors for water quality monitoring. Nat Nanotechnol 13:651–660. https://doi.org/10.1038/s41565-018-0209-9

Vu QK, Tran QH, Vu NP, Anh TL, Le Dang TT, Matteo T, Nguyen THH (2021) A label-free electrochemical biosensor based on screen-printed electrodes modified with gold nanoparticles for quick detection of bacterial pathogens. Materials Today Communications. https://doi.org/10.1016/j.mtcomm.2020.101726

World Health Organization (WHO) (2014) Water Quality and Health. Drinking water chlorination–A review of disinfection practices and issues. https://waterandhealth.org/safe-drinking-water/wp/ Accessed on 1 January 2023.

World Health Organization (2000) The world health report 2000: health systems: improving performance. World Health Organization, pp 144–200.

Wu B, Kuang Y, Zhang X, Chen J (2011) Noble metal nanoparticles/carbon nanotubes nanohybrids synthesis and applications. Nano Today 6:75–90. https://doi.org/10.1016/j.nantod.2010.12.008

Xu S, Zhang Y, Dong K, Wen J, Zheng C, Zhao S (2017) Electrochemical DNA biosensor based on graphene oxide-chitosan hybrid nanocomposites for detection of Escherichia coli O157: H7. Int J Electrochem Sci 12:3443–3458. https://doi.org/10.20964/2017.04.16

Xu W, Yang T, Liu S, Du L, Chen Q, Li X, Dong J, Zhang Z, Lu S, Gong Y, Zou L, Liu Y, Tan X (2022) Insights into the synthesis, types, and application of Iron Nanoparticles: the overlooked significance of environmental effects. Environ Inter. https://doi.org/10.1016/j.envint.2021.106980

Yabuki A, Tanaka S (2011) Oxidation behavior of copper nanoparticles at low temperature. Mater Res Bull 46:2323–2327. https://doi.org/10.1016/j.materresbull.2011.08.043

Yan Z, Yang M, Wang Z, Zhang F, Xia J, Shi G, Xia L, Li Y, Xia Y, Xia L (2015) A label-free immunosensor for detecting common acute lymphoblastic leukemia antigen (CD10) based on gold nanoparticles by quartz crystal microbalance. Sensor Actuat B 210:248–253. https://doi.org/10.1016/j.snb.2014.12.104

Yoshitomi T, Hayashi M, Oguro T, Kimura K, Wayam F, Furusho H, Yoshimoto K (2020) Binding and structural properties of DNA aptamers with VEGF-A-mimic activity. Molecular Therapy-Nucleic Acids 19:1145–1152. https://doi.org/10.1016/j.omtn.2019.12.034

Yu L, Li N (2019) Noble metal nanoparticles-based colorimetric biosensor for visual quantification: A mini-review. Chemosensors 7:53. https://doi.org/10.3390/chemosensors7040053

Yu T, Xu H, Zhao Y, Han Y, Zhang Y, Zhang J, Ge J (2020) Aptamer-based high throughput colorimetric biosensor for detection of Staphylococcus aureus. Sci Rep 10:1–6. https://doi.org/10.1038/s41598-020-66105-7

Zheng Y, Wang Y, Yang X (2011) Aptamer-based colorimetric biosensing of dopamine using unmodified gold nanoparticles. Sens Actuators, B Chem 156:95–99. https://doi.org/10.1016/j.snb.2011.03.077

Zheng L, Qi P, Zhang D (2018) A simple, rapid, and cost-effective colorimetric assay based on the 4-mercapto phenylboronic acid-functionalized silver nanoparticles for bacteria monitoring. Sens Actuators, B Chem 260:983–989. https://doi.org/10.1016/j.snb.2018.01.115

Zhong X, Chai YQ, Yuan R (2014) A novel strategy for the synthesis of hollow gold nanosphere and its application in electrogenerated chemiluminescence glucose biosensor. Talanta 128:9–14. https://doi.org/10.1016/j.talanta.2014.03.07

Zienkiewicz-Strzalka M, Derylo-Marczewska A, Kozakevych RB (2018) Silica nanocomposites based on silver nanoparticles-functionalization and pH effect. Appl Nanosci 8:1649–1668. https://doi.org/10.1007/s13204-018-0837-2